Auroral ion precipitation at Jupiter:

Predictions for Juno

by N. Ozak, T. E. Cravens, and D. R. Schultz

2013

Auroral ion precipitation at Jupiter: Predictions for Juno

N. Ozak,[1,2] T. E. Cravens,[1] and D. R. Schultz[3]

Received 10 June 2013; revised 29 July 2013; accepted 1 August 2013; published 22 August 2013.

[1] The spatially localized and highly variable polar cap emissions at Jupiter are part of a poorly understood current system linking the ionosphere and the magnetopause region. Strong X-ray emission has been observed from the polar caps and has been explained by the precipitation of oxygen and sulfur ions of several MeV energy. The present paper presents results of an extended model of the ion precipitation process at Jupiter. Specifically, we add to a previous model a more complete treatment of ionization of the atmosphere, generation of secondary electron fluxes and their escape from the atmosphere, and generation of downward field-aligned currents. Predictions relevant to observations by the upcoming NASA Juno mission are made, namely the existence of escaping electrons with energies from a few eV up to 10 keV, auroral H_2 band emission rates of 80 kR, and downward field-aligned currents of at least 2 MA.
Citation: Ozak, N., T. E. Cravens, and D. R. Schultz (2013), Auroral ion precipitation at Jupiter: Predictions for Juno, *Geophys. Res. Lett.*, *40*, 4144–4148, doi:10.1002/grl.50812.

1. Introduction

[2] Auroral X-ray emissions from Jupiter have been observed over the past 20 years by the Röntgen satellite, Chandra X-ray Observatory (CXO), and XMM-Newton [e.g., *Waite et al.*, 1994; *Gladstone et al.*, 2002; *Elsner et al.*, 2005; *Branduardi-Raymont et al.*, 2007, 2008]. From these observations, it is known that Jupiter emits about 1 GW of X-ray power from each hemisphere with emission originating poleward of the main auroral oval [*Elsner et al.*, 2005]. The observed X-ray spectra indicate that the emission is due to radiative relaxation following charge exchange of precipitating, initially very energetic (1–2 MeV/u), oxygen and sulfur ions slowed during their traversal of the upper atmosphere [*Hui et al.*, 2009, 2010; *Ozak et al.*, 2010].

[3] The X-ray aurora is thought to be associated with downward field-aligned currents [*Cravens et al.*, 2003]. The precipitating ions must be accelerated to MeV/u energies in order to produce high charge-state ions whose transitions are in the X-ray part of the spectrum because only at such energies will the stripping and charge exchange cross sections for collisions with H_2 targets have the right ratio [cf. *Cravens et al.*, 2003]. The accelerating potential will also increase the precipitating fluxes as given by the Knight relation [*Knight*, 1973]. *Bunce et al.* [2004] suggested that the ion acceleration and fluxes are due to magnetic reconnection at the dayside magnetopause, and they estimate accelerating voltages of 10–100 kV above regions of upward current and 0.5–5 MV above regions of downward current on the magnetospheric side of the open/closed field line boundary. The polar cap location of the X-ray aurora probably maps out to the outer magnetosphere (or magnetopause) [*Bunce et al.*, 2004] where heavy ion fluxes at the required energetics are quite low [*Mauk et al.*, 2002]. Hence, ion acceleration by a field-aligned potential appears to be necessary [*Cravens et al.*, 2003].

[4] The X-ray auroral morphology is complex. For example, observations by CXO showed a ∼45 min pulsation period X-ray hot spot [*Gladstone et al.*, 2002]. However, this pulsation was absent in later XMM-Newton and CXO observations [*Elsner et al.*, 2005; *Branduardi-Raymont et al.*, 2007]. In contrast, the auroral emission in the main oval is relatively steady and intense (about 0.1–1 MR, 1 Rayleigh (R) = 10^6 photons/cm^2/s) and has been successfully explained by downward precipitation of 20–100 keV electrons associated with the upward field-aligned current system driven by outward mass transport and corotation lag [*Hill*, 2001; *Cowley and Bunce*, 2001]. The current systems associated with the polar cap have received less attention, as have downward current regions in general. In the polar cap, the solar wind interaction (i.e., the Dungey cycle) will play an important role in addition to the Vasyliunas cycle. The total UV emission from the poles is generally less intense than main oval emission, but can occasionally be very intense, highly localized, and time dependent (e.g., the UV flares described by *Waite et al.* [2001] and *Bonfond et al.* [2011]). Nevertheless, the source of the emission and its temporal variation is not well understood, as well as its connection to the X-ray emission, if any.

[5] Earlier work to model Jovian ion precipitation emphasized the X-ray emission rather than the resulting atmospheric effects of this type of aurora [*Kharchenko et al.*, 1998, 2006, 2008; *Hui et al.*, 2009, 2010]. *Horanyi et al.* [1988] estimated the energy distribution of secondary electrons due to oxygen ion precipitation, but only included low oxygen charge states. In the present work, we extend our previous model of X-ray producing ion precipitation on Jupiter and consider its consequences for magnetosphere-ionosphere coupling. We calculate secondary electron fluxes using new ion-molecule data, field-aligned currents, auroral airglow emission rates, and ionization rates, all of which are useful for interpretation of observations made by the NASA Juno mission. The primary ion fluxes and the associated secondary electron fluxes create currents that, at least locally, link Jovian auroral X-ray emission to the polar cap part of the magnetosphere-ionosphere current system and to the Jovian magnetospheric dynamics overall.

[1]Department of Physics and Astronomy, University of Kansas, Lawrence, Kansas, USA.
[2]Now at Department of Earth and Planetary Sciences, Weizmann Institute of Science, Rehovot, Israel.
[3]Department of Physics, University of North Texas, Denton, Texas, USA.

Corresponding author: N. Ozak, Department of Earth and Planetary Sciences, Weizmann Institute of Science, Rehovot 76100q, Israel. (nataly.ozak@weizmann.ac.il)

0094-8276/13/10.1002/grl.50812

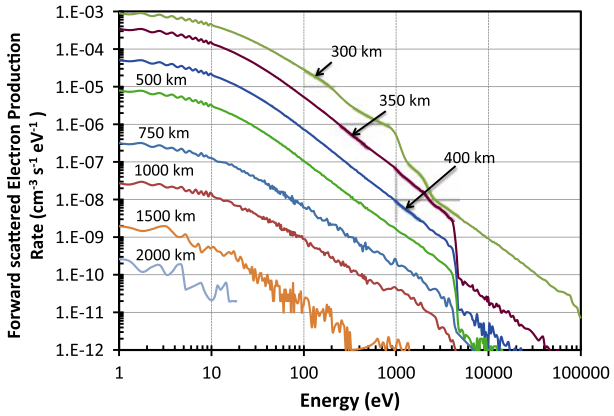

Figure 1. Secondary electron production rates at different altitudes in the atmosphere due to the precipitation of a single oxygen ion/cm^2/s with an incident energy of 2 MeV/u at the top of the atmosphere (energy flux = 32 MeV/cm^2/s). Only the forward scattered electrons are shown here. The high energy electron tails are due to secondary electrons from stripping (i.e., electron loss) collisions of O ions with H_2.

2. Effects of Auroral Ion Precipitation

[6] The ion precipitation Monte Carlo model of *Ozak et al.* [2010] was used here but extended to include secondary electron production. We adopt the Jovian neutral atmosphere presented by *Maurellis and Cravens* [2001], based on Galileo probe data [*Seiff et al.*, 1996, 1997] and remote observations [*Sada et al.*, 1998], also used in the previous ion precipitation model [*Ozak et al.*, 2010]. A detailed description of the numerical model for oxygen ion precipitation including secondary electron production will be described in a future paper. Ion (O^{q+}, $q = 0, 1, \ldots 8$) collisions with atmospheric H_2 molecules can have different outcomes as follows:

$$O^{q+} + H_2 \rightarrow \begin{cases} O^{q+} + H_2^+ + e & \text{Single Ionization} \\ O^{q+} + 2H^+ + 2e & \text{Double Ionization} \end{cases} \quad (1a)$$

$$O^{q+} + H_2 \rightarrow \begin{cases} O^{(q-1)+} + H_2^+ & \text{Charge Exchange} \\ O^{(q-1)+} + 2H^+ + e & \text{Transfer Ionization} \\ O^{(q-1)+} + 2H^+ + e & \text{Double Capture-Autoionization} \end{cases} \quad (1b)$$

$$O^{q+} + H_2 \rightarrow \begin{cases} O^{(q+1)} + H_2^* + e & \text{Single Stripping} \\ O^{(q+2)} + H_2^* + 2e & \text{Double Stripping} \end{cases} \quad (1c)$$

The model keeps track of these electrons and how they deposit their energy in the atmosphere. Similar processes involving the other principal species responsible for the auroral X-ray emission, sulfur ion precipitation, will be considered in future work.

2.1. Ion and Electron Production Rates

[7] Previous models [*Kharchenko et al.*, 2008; *Hui et al.*, 2010; *Ozak et al.*, 2010] showed that ions with initial energies between 1 and 2 MeV/u are most efficient in producing X-ray emission. Here we adopt incident oxygen ions with energies of 1, 1.5, and 2 MeV/u as typical of this range and then inject 10,000–15,000 ions at the top of the atmosphere to build enough statistics. The ions start with a low charge state ($q = 2$) typical of the outer magnetosphere. The Monte Carlo simulation then yields rates of production of secondary electrons and H^+ and H_2^+ ions. In particular, the Monte Carlo primary ion part of our model keeps track of ion energy and charge state as the ion precipitates into the atmosphere and also bookkeeps the number of ionization events (i.e., H_2^+ and H^+ production) as well as secondary electron production from ionization and stripping collisions (equation (1)).

[8] Figure 1 shows the downward electron production rate due to a single oxygen ion with an initial energy of 2 MeV/u. We find that the bulk of secondary electrons have energies less than 100 eV. Most of the electrons originate from ionizing collisions. Stripping collisions produce more energetic secondary electrons since they are ejected in the frame of the moving projectile, and these are evident as a high energy tail in the electron energy distribution. The highest production rate is at the lowest altitudes reached by the ions, since the atmosphere is denser and the collisions more frequent. The backward (upward) electron production rates (not shown in the figure) are up to an order of magnitude smaller than the forward production rates, and the high energy tail is not present, since the secondary electrons produced in stripping collisions are predominantly produced in the forward direction. Higher initial ion energies correspond to a peak ion production rate located deeper in the atmosphere.

[9] While the area of emission on the polar cap is difficult to determine given the large time variability, we use CXO observations from 2003 [*Elsner et al.*, 2005, Figure 7] to estimate that the north aurora comes from an area of $\sim 2 \times 10^{18}$ cm^2 and the south aurora from an area of $\sim 1 \times 10^{19}$ cm^2. The north aurora emissions appear to be concentrated in a so-called "hot spot," while the south aurora emissions are more diffuse. *Elsner et al.* [2005] derived an X-ray power for the northern hot spot of 0.68 GW, so we approximate the total emitted power at each polar region (north or south) to be ~1 GW. For a 2 MeV/u oxygen ion, *Ozak et al.* [2010] estimated an X-ray efficiency of 7×10^{-5} and therefore a global ion input power of 10^{13} W is needed to produce ~ 1 GW of X-ray power. This corresponds to a total incident ion input of 2×10^{24} ions/s or for the north auroral region

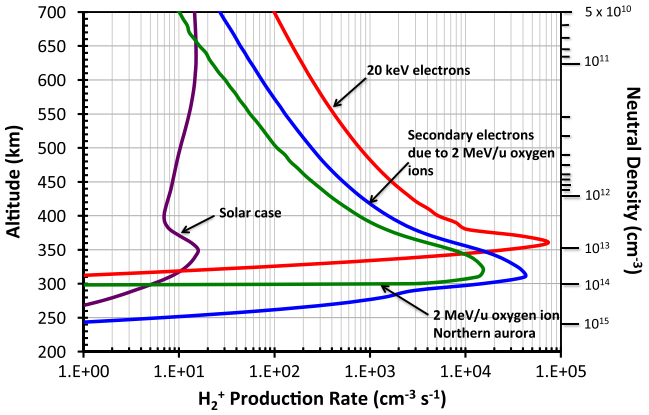

Figure 2. H_2^+ production rates as a function of altitude for these cases: (1) photoionization and subsequent photoelectron ionization (solar radiation, purple line); (2) 20 keV monoenergetic electrons with an input flux of 10 ergs/cm^2/s (red line); (3) 2 MeV/u oxygen ions giving rise to the northern X-ray aurora (green line); and (4) secondary electrons (only) from the primary oxygen ion precipitation (blue line).

Table 1. Column Ion-Production Rates and Airglow Emission Rates[a]

Ion Produced	2 MeV/u (North)	2 MeV/u (South)	20 keV Electrons	Solar Radiation
Production rate	($cm^{-2}s^{-1}$)	($cm^{-2}s^{-1}$)	($cm^{-2}s^{-1}$)	($cm^{-2}s^{-1}$)
H_2^+	3×10^{11}	5×10^{10}	2×10^{11}	1×10^{9}
H^+	7×10^{10}	1×10^{10}	1×10^{10}	2×10^{8}
He^+	1×10^{10}	2×10^{9}	1×10^{10}	4×10^{7}
CH_4^+	9×10^{8}	2×10^{8}	7×10^{8}	1×10^{8}
Lyman bands (direct excit.)	7×10^{10}	1×10^{10}	7×10^{10}	2×10^{8}
Lyman bands (cascade)	8×10^{9}	2×10^{9}	6×10^{9}	2×10^{7}
Werner bands	6×10^{10}	1×10^{10}	6×10^{10}	1×10^{8}
Lyman alpha (from H_2 diss.)	2×10^{10}	2×10^{9}	1×10^{10}	3×10^{7}
Lyman alpha (from H)	5×10^{7}	1×10^{7}	1×10^{8}	1×10^{7}

[a]Only the main ion species are shown here. The cases included are (1) the north and (2) south ion aurora due to 2 MeV/u oxygen ions (primary and secondary ionization), (3) 20 keV primary auroral electrons with an incident energy flux of 10 ergs/cm^2/s, and (4) solar radiation (photoionization and photoelectron contributions). A solar zenith angle of 0° was assumed.

an ion flux of 10^6 ions/cm^2/s. For the south polar region, the flux is about 2×10^5 ions/cm^2/s. Fluxes measured in the outer magnetosphere are low, especially for such high energy ions. However, the field-aligned potential needed to accelerate the ions to high energies will also increase the ion flux to the planet (see *Cravens et al.* [2003] for flux estimates).

[10] The electron two-stream part of our model next takes the secondary electron production rates and determines their energy deposition (i.e., ionization and airglow). Transport of secondary electrons along magnetic field lines is taken into account. We also model photoionization by solar radiation and determine the resulting photoelectron fluxes [see *Maurellis and Cravens*, 2001]. Figure 2 shows calculated H_2^+ production rates for four cases. Dissociative ionization (H^+) is also included, leading some H_2^+ ions to end as H^+ in the bookkeeping. The first case (purple line) is ion production rate from solar radiation, and a H_2^+ column production rate of 1×10^9 $cm^{-2}s^{-1}$ is obtained (Table 1). The second case (red line) is the ionization rate due to a 20 keV incident monoenergetic electron beam with a typical input energy flux of 10 erg/cm^2/s [*Waite et al.*, 1983] for which we obtain a column ionization rate of 2×10^{11} $cm^{-2}s^{-1}$. The third case (green line) is the ion production rate due to 2 MeV/u oxygen ions precipitating in the north polar region with an ion flux of 10^6 ions/cm^2/s (consisting only of "primary" ionization by the ions). The fourth case (blue line) is the ion production rate due to ionization collisions by the secondary electrons from the ion aurora (secondary ionization). The total column ionization rate due to the ion aurora (primary and secondary ionization) is 3×10^{11} $cm^{-2}s^{-1}$ for the north and 5×10^{10} $cm^{-2}s^{-1}$ for the south. Thus, ion and electron precipitation can generate comparable atmospheric ionization rates.

2.2. Electron Energy Spectra

[11] Secondary electron fluxes up and down the magnetic field line are another model output. For example, Figure 3 shows upward electron flux versus altitude for a single incident oxygen ion with an initial energy of 2 MeV/u. The figure also shows that below 1000 km, lower energy electrons (e.g., 10 eV) are almost isotropic (equal up and down fluxes) and that the electron flux reaches a steady value for altitudes above ~1500 km. At these high altitudes with low neutral densities, the probability of an electron collision becomes small. The upward electron flux at the top of the atmosphere (or escape flux) is important for magnetosphere-ionosphere coupling and should be measurable by the Juno spacecraft.

[12] Figure 4 compares the calculated escaping electron fluxes (i.e., upward flux at 3000 km in our model) for four different cases. The purple curve shows the escaping photoelectron flux (i.e., induced by solar radiation), which, at low electron energies (E < 25 eV), can be large during the daytime. The red curve shows the escape fluxes due to a primary 20 keV electron aurora with an input energy flux of 10 erg/cm^2/s. Note that we validated our two-stream model for auroral electrons by comparing with previous electron aurora models [*Waite et al.*, 1983; *Grodent and Gérard*, 2001]. The figure also shows the calculated spectra of escaping electrons for the ion aurora in the north and south polar regions for 2 MeV/u oxygen ions. The electron escape due to the ion aurora is smaller than that of the electron aurora. In the ion aurora, most electrons are produced deeper in the atmosphere and have more difficulty escaping.

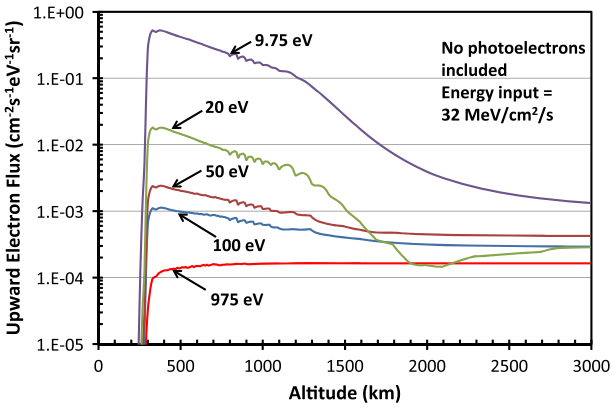

Figure 3. Upward electron fluxes as a function of altitude for specific electron energies as labeled in the figure. The fluxes are due to secondary electrons from a single 2 MeV/u oxygen ion (energy flux = 32 MeV/cm^2/s). There is no other external input of electrons (i.e., no magnetospheric electron beams or photoelectrons).

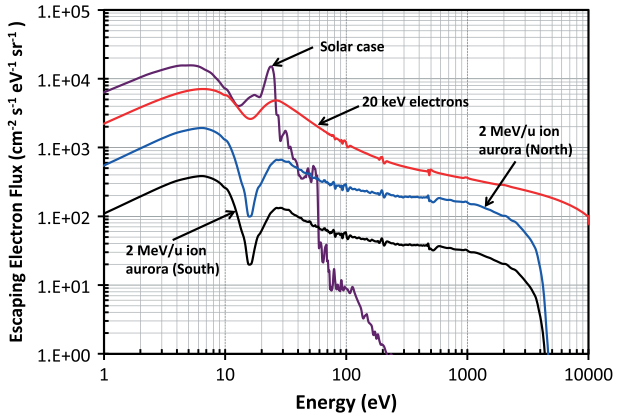

Figure 4. Escape flux of electrons (i.e., upward electron fluxes at the top of the atmosphere, z = 3000 km) as a function of electron energy. Four different cases: as labeled and discussed in the text.

3. Field-Aligned Current

[13] Ion precipitation is associated with downward field-aligned currents [*Cravens et al.*, 2003; *Bunce et al.*, 2004] and is due to both the primary ions and to escaping secondary electrons. For an input of a single 1 MeV/u/cm^2/s ion into the atmosphere, we calculate that only one electron/cm^2/s escapes upward. As we increase the initial ion energy at the top of the atmosphere to 2 MeV/u, this number only increases to 1.5 electrons/cm^2/s. Most secondary electrons are created deep in the atmosphere and are unable to escape. For a total 2 MeV/u ion flux of 10^6 ions/cm^2/s (north aurora), we calculate that a flux of $\sim 1.5 \times 10^6$ electrons/cm^2/s escapes with a current density of $\sim 3 \times 10^{-13}$A/cm^2. Using the estimated areas for the X-ray aurora, this gives a downward current of 0.6 MA for the north and 0.5 MA for the south. Our estimated incident ion flux (2×10^{24} ions/s) globally for a 1 GW X-ray aurora gives a downward current of ~0.7 MA. Together, the total downward field-aligned current is about 2 MA. *Cravens et al.* [2003] roughly estimated this to be 8 MA. Note that ions with primary energies less than 1 MeV/u may also be present, produced by the solar wind interaction [*Bunce et al.*, 2004], and they will generate ionization, currents, and airglow, but much less X-ray emission, so our downward current estimate is only a lower limit.

4. Implications of Auroral Precipitation: Airglow

[14] In addition to ionization, either electron or ion precipitation generates airglow emission. We have carried out preliminary calculations for the ion aurora assuming that the secondary electrons dominate the airglow production. A more complete model will be described in a future paper. We have also not yet considered optical depth effects. Table 1 shows calculated total H_2 Lyman and Werner band airglow production rates. H Lyman alpha production is also included. The peak ion production rate is at a lower altitude for the 2 MeV/u oxygen aurora than it is for the 20 keV electron aurora, which may give rise to higher opacity effects to the airglow emissions.

[15] Lyman and Werner band intensities together, due to the secondary electron contribution from the ion precipitation, are 60–80 kR in the north and 10–20 kR in the south. These intensities (uncorrected for optical depth) are comparable to observed UV intensities for primary electron precipitation (25–130 kR for faint regions and 250 kR for bright regions in the polar cap [*Kim et al.*, 1995]). Intensities in the main auroral oval are much brighter (50 kR to 1 MR at its brightest) [*Grodent et al.*, 2003].

5. Predictions for the Juno Mission and Summary

[16] The NASA Juno spacecraft will arrive at Jupiter in July 2016 (see http://www.nasa.gov/mission_pages/juno/main) and its suite of instruments is ideal for making auroral observations that can be compared to predictions of the present X-ray/electron emission model and interpreted by it. The Juno orbits are polar, passing through auroral magnetic field lines at distances of a few thousand km above the cloud tops. Its instruments are capable of detecting ions and electrons moving up and down the field lines. In particular, measurement of energetic (many MeV) downward oxygen and sulfur ions would definitively confirm the proposed X-ray emission mechanism [cf. *Cravens et al.*, 2003; *Ozak et al.*, 2010]. We have also predicted outgoing suprathermal electron fluxes for both ion and electron precipitation (Figure 4), and the Jovian Energetic-particle Detector Instrument (JEDI) and Jovian Auroral Distribution Experiment (JADE) instruments will be able to measure such fluxes. Some instrument-specific observations testing the present model are listed below:

[17] 1. Ultraviolet spectrometer: Do UV emissions correlate spatially and temporally with X-ray measurements? Do the intensities agree with the predictions of the present model given the X-ray luminosity?

[18] 2. JEDI: Most importantly, are downward several MeV heavy ions observed a few Jovian radii above the polar caps with sufficient flux to generate the observed X-ray emission? Neither the Pioneer, Voyager, or Galileo spacecraft had trajectories/orbits that would have permitted such ions to be measured. Similarly, are primary downward electron fluxes detected in the polar cap and over the main oval?

[19] 3. JADE: We predict that upward electron fluxes with energies between 100 eV and 100 keV should be present in the polar cap. Such observations can be used to test our predictions of escaping electrons from electron and ion precipitation (Figure 4). However, if Juno is above the acceleration region, the upward electron energies will be several MeV. Energetic electron measurements on the Pioneer and Voyager missions [e.g., *Schardt and Goertz*, 1983] did not indicate discrete MeV electron features in the outer magnetosphere. However, the required acceleration regions are quite localized on the planet and might not always be present in the outer magnetosphere. Nevertheless, the Ulysses spacecraft did detect discrete MeV electron events on high-latitude magnetic field lines in the outer magnetosphere [*McKibben et al.*, 1993; *Karanikola et al.*, 2004; *Zhang et al.*, 1995]. Also, *MacDowall et al.* [1993] suggested that observed QP-40 Jovian radio emissions could be explained by relativistic electrons above the poles. For comparison, the outward flux of electrons for ion precipitation (Figure 4) is $\approx 3 \times 10^6$ cm^{-2}s^{-1} which would give a roughly 10 MeV electron flux of $\approx 2 \times 10^4$ cm^{-2}s^{-1} just above an acceleration region located at about 5 R_J and about 20 cm^{-2}s^{-1} near the equator. Measured fluxes of this energy electrons (or higher)

in the radiation belt are $\approx 10^7$ cm^{-2}s^{-1} [*Schardt and Goertz*, 1983] but in the outer magnetosphere are only ~10–100 cm^{-2}s^{-1}, which is comparable to the ion aurora outward beam electron flux.

[20] When interpreting Juno measurements, it is important to recognize that ion populations related to the X-ray emission process found above the acceleration region will have low energies, while electron populations measured in this region are expected to be highly energetic. On the other hand, if the observations are below the acceleration region, we would expect to see a high flux of energetic ions and low energy electrons. It is important to map these populations to the ionosphere as they may provide a better understanding of the dynamic polar auroral region and the relation between the X-ray and UV emissions seen there.

[21] **Acknowledgments.** The authors wish to thank NASA for their support via Planetary Atmospheres grant NNX10AB86G.

[22] The Editor thanks two anonymous reviewers for their assistance in evaluating this paper.

References

Bonfond, B., M. F. Vogt, J.-C. Gérard, D. Grodent, A. Radioti, and V. Coumans (2011), Quasi-periodic polar flares at Jupiter: A signature of pulsed dayside reconnections?, *Geophys. Res. Lett.*, *38*, L02104, doi:10.1029/2010GL045981.

Branduardi-Raymont, G., A. Bhardwaj, R. F. Elsner, G. R. Gladstone, G. Ramsay, P. Rodriguez, R. Soria, J. H. Waite Jr., and T. E. Cravens (2007), A study of Jupiter's aurorae with XMM-Newton, *Astron. Astrophys.*, *463*, 761–774, doi:10.1051/0004-6361:20066406.

Branduardi-Raymont, G., R. F. Elsner, M. Galand, D. Grodent, T. E. Cravens, P. Ford, G. R. Gladstone, and J. H. Waite (2008), Spectral morphology of the X-ray emission from Jupiter's aurorae, *J. Geophys. Res.*, *113*, A02202, doi:10.1029/2007JA012600.

Bunce, E. J., S. W. H. Cowley, and T. K. Yeoman (2004), Jovian cusp processes: Implications for the polar aurora, *J. Geophys. Res.*, *109*, A09S13, doi:10.1029/2003JA010280.

Cowley, S. W. H., and E. J. Bunce (2001), Origin of the main auroral oval in Jupiter's coupled magnetosphere-ionosphere system, *Planet. Space. Sci.*, *49*, 1067–1088.

Cravens, T. E., J. H. Waite, T. I. Gombosi, N. Lugaz, G. R. Gladstone, B. H. Mauk, and R. J. MacDowall (2003), Implications of Jovian X-ray emission for magnetosphere-ionosphere coupling, *J. Geophys. Res.*, *108*(A12), 1465, doi:10.1029/2003JA010050.

Elsner, R. F., et al. (2005), Simultaneous Chandra X-ray, Hubble Space Telescope ultraviolet, and Ulysses radio observations of Jupiter's aurora, *J. Geophys. Res.*, *110*, A01207, doi:10.1029/2004JA010717.

Gladstone, G. R., et al. (2002), A pulsating auroral X-ray hot spot on Jupiter, *Nature*, *415*(6875), 1000–1003.

Grodent, D., and J. Gérard (2001), A self-consistent model of the Jovian auroral thermal structure, *J. Geophys. Res.*, *106*, 12,933–12,952, doi:10.1029/2000JA900129.

Grodent, D., J. T. Clarke, J. Kim, J. H. Waite, and S. W. H. Cowley (2003), Jupiter's main auroral oval observed with HST-STIS, *J. Geophys. Res.*, *108*(A11), 1389, doi:10.1029/2003JA009921.

Hill, T. W. (2001), The Jovian auroral oval, *J. Geophys. Res.*, *106*, 8101–8108, doi:10.1029/2000JA000302.

Horanyi, M., T. E. Cravens, and J. H. Waite Jr. (1988), The precipitation of energetic heavy ions into the upper atmosphere of Jupiter, *J. Geophys. Res.*, *93*, 7251–7271, doi:10.1029/JA093iA07p07251.

Hui, Y., D. R. Schultz, V. A. Kharchenko, P. C. Stancil, T. E. Cravens, C. M. Lisse, and A. Dalgarno (2009), The ion-induced charge-exchange X-ray emission of the Jovian auroras: Magnetospheric or solar wind origin?, *Astrophys. J.*, *702*, L158–L162, doi:10.1088/0004-637X/702/2/L158.

Hui, Y., D. R. Schultz, V. A. Kharchenko, A. Bhardwaj, G. Branduardi-Raymont, P. C. Stancil, T. E. Cravens, C. M. Lisse, and A. Dalgarno (2010), Comparative analysis and variability of the Jovian X-ray spectra detected by the Chandra and XMM-Newton observatories, *J. Geophys. Res.*, *115*, A07102, doi:10.1029/2009JA014854.

Karanikola, I., M. Athanasiou, G. Anagnostopoulos, G. Pavlos, and P. Preka-Papadema (2004), Quasi-periodic emissions (1580 min) from the poles of Jupiter as a principal source of the large-scale high-latitude magnetopause boundary layer of energetic particles, *Planet. Space Sci.*, *52*(5–6), 543–559, doi:10.1016/j.pss.2003.10.002.

Kharchenko, V., W. Liu, and A. Dalgarno (1998), X-ray and EUV emission spectra of oxygen ions precipitating into the Jovian atmosphere, *J. Geophys. Res.*, *103*, 26,687–26,698, doi:10.1029/98JA02395.

Kharchenko, V., A. Dalgarno, D. R. Schultz, and P. C. Stancil (2006), Ion emission spectra in the Jovian X-ray aurora, *Geophys. Res. Lett.*, *33*, L11105, doi:10.1029/2006GL026039.

Kharchenko, V., A. Bhardwaj, A. Dalgarno, D. R. Schultz, and P. C. Stancil (2008), Modeling spectra of the north and south Jovian X-ray auroras, *J. Geophys. Res.*, *113*, A08229, doi:10.1029/2008JA013062.

Kim, Y. H., J. J. Caldwell, and J. L. Fox (1995), High-resolution ultraviolet spectroscopy of Jupiter's aurora with the Hubble Space Telescope, *Astrophys. J.*, *447*, 906–914, doi:10.1086/175928.

Knight, S. (1973), Parallel electric fields, *Planet. Space Sci.*, *21*, 741–750, doi:10.1016/0032-0633(73)90093-7.

MacDowall, R. J., M. L. Kaiser, M. D. Desch, W. M. Farrell, R. A. Hess, and R. G. Stone (1993), Quasiperiodic Jovian radio bursts: Observations from the Ulysses radio and plasma wave experiment, *Planet. Space Sci.*, *41*, 1059–1072, doi:10.1016/0032-0633(93)90109-F.

Mauk, B. H., B. J. Anderson, and R. M. Thorne (2002), Magnetosphere-ionosphere coupling at Earth, Jupiter, and beyond, in *Atmospheres in the Solar System: Comparative Aeronomy*, vol. 130, edited by M. Mendillo et al., pp. 97–114, American Geophysical Union, Washington, D. C., doi:10.1029/130GM07.

Maurellis, A. N., and T. E. Cravens (2001), Ionospheric effects of Comet Shoemaker-Levy 9 impacts with Jupiter, *Icarus*, *154*, 350–371, doi:10.1006/icar.2001.6709.

McKibben, R., J. Simpson, and M. Zhang (1993), Impulsive bursts of relativistic electrons discovered during Ulysses' traversal of Jupiter's dusk-side magnetosphere, *Planet. Space Sci.*, *41*(11–12), 1041–1058, doi:10.1016/0032-0633(93)90108-E.

Ozak, N., D. R. Schultz, T. E. Cravens, V. Kharchenko, and Y.-W. Hui (2010), Auroral x-ray emission at Jupiter: Depth effects, *J. Geophys. Res.*, *115*, A11306, doi:10.1029/2010JA015635.

Sada, P. V., G. L. Bjoraker, D. E. Jennings, G. H. McCabe, and P. N. Romani (1998), Observations of CH_4, C_2H_6, and C_2H_2 in the stratosphere of Jupiter, *Icarus*, *136*, 192–201, doi:10.1006/icar.1998.6021.

Schardt, A. W., and C. K. Goertz (1983), *High-Energy Particles*, pp. 157–196, Planetary Science, Cambridge.

Seiff, A., et al. (1996), Structure of the atmosphere of Jupiter: Galileo probe measurements, *Science*, *272*, 844–845, doi:10.1126/science.272.5263.844.

Seiff, A., et al. (1997), Thermal structure of Jupiter's upper atmosphere derived from the Galileo probe, *Science*, *276*, 102–104, doi:10.1126/science.276.5309.102.

Waite, J. H., T. E. Cravens, J. Kozyra, A. F. Nagy, S. K. Atreya, and R. H. Chen (1983), Electron precipitation and related aeronomy of the Jovian thermosphere and ionosphere, *J. Geophys. Res.*, *88*, 6143–6163, doi:10.1029/JA088iA08p06143.

Waite, J. H., et al. (2001), An auroral flare at Jupiter, *Nature*, *410*(6830), 787–789.

Waite, J. H., Jr., et al. (1994), ROSAT observations of the Jupiter aurora, *J. Geophys. Res.*, *99*, 14,799–14,809, doi:10.1029/94JA01005.

Zhang, M., R. B. McKibben, J. A. Simpson, S. W. H. Cowley, K. Staines, J. D. Anglin, R. G. Marsden, T. R. Sanderson, and K.-P. Wenzel (1995), Impulsive bursts of energetic particles in the high-latitude dusk-side magnetosphere of Jupiter, *J. Geophys. Res.*, *100*, 19,497–19,512, doi:10.1029/95JA02099.